Modeling and conditional integrator control of an unmanned aerial vehicle for airlaunch

Cuong Nguyen Van, Gilney Damm

Modeling and Conditional Integrator Control of an Unmanned Aerial Vehicle for Airlaunch

Van Cuong Nguyen and Gilney Damm

***Abstract*— A satellite launching procedure known as airlaunch is modeled and simulated at the staging phase, where a reusable unmanned aerial vehicle airlaunches a second (rocket) stage. This allows to study the effects of the split phase on the stability of the airlaunch system. A robust conditional integrator controller is designed with the objective of stabilizing the system during and after the airlaunch. The controller is indeed able to assure system stability for rather large disturbances. Performance of the proposed control algorithm is illustrated through simulations.**

I. Introduction

Satellites launching is a strategical activity today. Launchers are able to carry from micro-satellites of some tens of kilograms up to 10 tons in the case of French Ariane 5 launcher. Recently new applications have called upon very small satellites, named nano-satellites, mostly used in groups (see [1]). These nano-satellites need a new class of launchers since launching implies in many fixed costs that are independent of the size and weight of the launched device. For this reason, the ratio price-per-kilogram launched in space becomes too high. A quite logical solution in this case would be to pack many small devices to be launched together. Unfortunately this implies many additional risks in the split phase and is not envisaged.

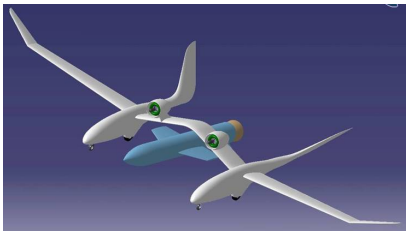

Fig. 1. Airlauch system: EOLE in PERSEUS project

A more efficient solution in this case is to use the procedure of airlaunch (see [13], [3]). It consists of using a two stages launching system (see Fig. 1). The first stage is composed of an air vehicle (manned or unmanned) that carries (inside, beneath or above) a launcher which constitutes the second stage. There are many advantages in airlaunch, mainly because there is no need for specific large non populated launching areas. The aerial vehicle takes-off from a standard runway and fly to open ocean, avoiding populated areas or ship and airplane paths. For this reason there is also a minimization of weather constraints, since the vehicle can fly to open sky, and as consequence the launch delay can be significantly shortened. Similarly, instead of waiting for specific launch windows (to attain desired orbits), the vehicle may be flown to a better suited launch point, with a better alignment with the desired orbit. The fact that the first stage is a reusable aerial vehicle allows a much smaller launching delay. In the same way, launching reuse time may be very short (one or two days). These characteristics provide great flexibility, and allow to deploy small satellites designed for specific tasks of communication or data gathering in real time for urgent situations.

Airlaunch provides the advantages of two stage launchers. The second (dropped) stage may use specific nozzles and propellants for the low outside atmospheric pressure at altitude (20 000 meters or 60000 feet). This is obtained without the complex, expensive and relatively dangerous high pressure ground-launched first stage that is replaced by the aerial vehicle. Most current airlaunch projects use standard or lightly modified airplanes as first stage. For example, there has been tests using F15, C17, B52, L-1011 in Rascal, QuickReach, Proteus, Pegasus projects.

It is important to remark that airplanes use the wing's lift force to fly. For this reason, higher (low altitude) air density benefit the flight while the aircraft uses standard fuel to keep flying. A first stage rocket would use a much more complex, dangerous and expensive fuel while in this higher air density. From a certain altitude, air density is too low to be useful for an airplane, while not representing anymore a drawback for rockets.

For all these reasons, French space agency, Center National d'Etudes Spatiales (CNES), started the project PERSEUS (Projet Etudiant de Recherche Spatiale Europen Universitaire et Scientifique), PERSEUS intends to use an unmanned aerial vehicle to fly the launcher to the desired drop point. There are many advantages in doing so, in first place safety since no human lives are involved during the delicate launching phase. In addition, since there is no need for life supporting devices, weight is restricted to the strict minimum. Finally, mission may take as long as necessary without human restrictions as tiredness.

That project aims in developing an airlaunch system that uses an Unmanned Aerial Vehicle (UAV) instead of a standard aircraft with a human pilot inboard. The current paper addresses its launching phase. It intends to introduce modeling and a robust controller for this delicate procedure. In fact, airlaunch may be very challenging since the rocket

Van Cuong Nguyen is with IBISC - Université d'Evry Val d'Essonne, Evry, France vancuong.nguyen@ibisc.fr

Gilney Damm is with IBISC - Université d'Evry Val d'Essonne, Evry, France gilney.damm@ibisc.fr

may be almost as heavy as the UAV. This means that the aircraft will instantaneously lose almost half of its mass. Current airlaunch systems present a much smaller ratio launcher/aircraft and rely on human pilot to stabilize the aircraft during and immediately after the launching instant. Unlike those systems, our airlaunch uses an UAV, and as consequence, the stabilization task is much more complex during and after the launching phase with a much more adverse mass ratio. In the best knowledge of authors, it does not exist an equivalent research line, and then there is no results in the literature considering this problem (modeling and control).

The paper is organized as follows: in section II, we describe the nonlinear mathematical system model, we illustrate some cases of non perfect separations during staging phase. A conditional integrator control design and its application to the full system model is discussed in section III. The paper is completed by computer simulations and conclusions.

II. Modeling

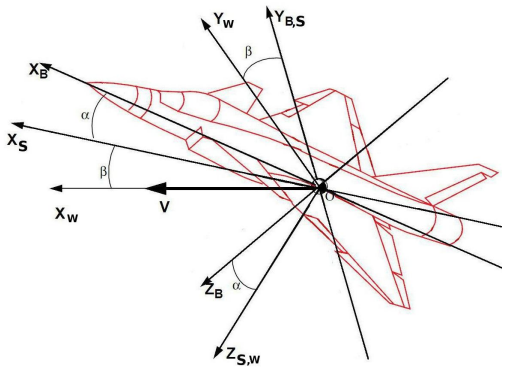

Fig. 2. Frames: Body fixed axes $OX_BY_BZ_B$, Stability axes $OX_SY_SZ_S$, Aerodynamic axes $OX_WY_WZ_W$

Modeling an air launch system and its separation phase is a difficult task which requires many data and informations about the real system. Since the UAV and launcher are yet not available, as well as its wind tunnel measurements, we have based our work on a F-16 aircraft (that already has been tested for manned airlaunch). We have also used it to verify in simulations the reactions of the system when modeling the air launch phase.

There are some authors studying related topics. In [10] and [8], it is studied the stage separation of a reusable booster from its down stage. The booster allows a stage separation at a high angle of attack and at supersonic speed. In this study, the aerodynamic inference effects are included. An aerodynamic separation of booster from the down stage vehicle is simulated by a private software SepSim.

In [11] and [12], a two stage reusable launch vehicle is studied at the stage separation by a new ConSep simulation tool. The ConSep tool is applied to simulation and analysis of stage maneuver of two stage to orbit Bimese reusable launch vehicle with aerodynamic database from the data of wind tunnel tests at the NASA Langley Research Center. In this simulation, the effects of variations in mass and inertia from their nominal values at staging are evaluated. The effects of the variations in mass and inertia on the aerodynamic coefficients of the launch vehicle are an important topic for study.

Unlike these authors, we suppose that the studied system is a set of a reusable launch vehicle and a down stage, whose mass is equivalent to half of the reusable launch vehicle's own mass. For the sake of simplicity, this set form a complete aircraft before air launching.

Depending on the position of the the down stage on the reusable airlaunch vehicle, the system will possibly changes its mass, inertia matrix, abscissa of center of the gravity and aerodynamic coefficients. For the following study, we take assumptions:

Assumption 2.1: The abscissa of center of the gravity of the down stage is identical to that of the reusable airlaunch vehicle. For this reason, there is no change in abscissa of center of the gravity after the airlaunch phase.

Assumption 2.2: The change in aerodynamic coefficients only affects drag and moments.

Airlaunch can be modeled as an hybrid system composed by two (or three) continuous models that are switched. These models represents the system before, (possible during) and after the separation phase. In the present work we have adopted this strategy, we have considered three phases, using two aircraft models.

1) before the separation $\rightarrow$ The first aircraft model (representing the UAV and the rocket) is in an stable operating condition
2) during the separation $\rightarrow$ a second aircraft model representing only the UAV, starting on the previous operating condition is disturbed by impulses on forces and moments. These disturbances are inside a time interval T_{int} and represent a not perfect separation. Furthermore the initial conditions, inherited from the first phase, are not an equilibrium point for the second aircraft model.
3) after the separation $\rightarrow$ the disturbances stop (UAV and rocket are not in physical contact anymore).

It can be shown that the effect of launching the rocket from the UAV impacts most the lift force, and the roll and pitch moments. We suppose that these perturbing force and moments are constant during interval T_{int}, and we represent then F_{z_p}, L_p and M_p for the perturbations on the lift force, on the roll moment and pitch moment respectively.

In the present work we will study a worst case of disturbance. We consider that the separation phase is not simultaneous in all links that attach the rocket and the UAV. For this reason, the rocket remains attached to one end of the UAV during T_{int}. We have then studied how long the disturbance could last and that the control algorithm could still stabilize the aircraft back.

We have then assumed that:

- the perturbation on lift force during T_{int} is equal the rocket's mass (times gravity), that means $F_{z_p} = mg$.

- the perturbation on pitch moment during T_{int} is $M_p = mgl_r/2$ where l_r is the rocket length.
- the perturbation on roll moment during T_{int} is small, because of the geometry of the rocket (thin and long).
- the model following the launch phase is that of an F-16. Its initial condition is the equilibrium point of the model previous the launch phase. This is taken as the F-16 model with twice the F-16's mass.

The model of the dynamic airlaunch after the split phase is described by the Newton-Euler's law in the aerodynamic axes $OX_WY_WZ_W$ in Fig. 2 (see [5],[17],[18]) i.e. the reference frame attached to the airspeed vector (V), because of the measurability of its state variables.

$$\left\{\begin{array}{l}
\dot{\alpha} = -\cos\alpha\tan\beta p + q - \sin\alpha\tan\beta r \\
-\frac{\sin\alpha}{mV\cos\beta}(T+F_x) + \frac{\cos\alpha}{mV\cos\beta}F_z \\
+\frac{g}{V\cos\beta}[\sin\alpha\cos\theta + \cos\alpha\cos\phi\cos\theta] \\
\dot{\beta} = \sin\alpha p - \cos\alpha r - \frac{\cos\alpha\sin\beta}{mV}[T+F_x] + \frac{\cos\beta}{mV}F_y \\
-\frac{\sin\alpha\sin\beta}{mV}F_z + \frac{g}{V}[\cos\alpha\sin\beta\sin\theta \\
+\cos\beta\cos\theta\sin\phi - \sin\alpha\sin\beta\cos\phi\cos\theta] \\
\dot{V} = \frac{\cos\alpha\cos\beta}{m}[T+F_x] + \frac{\sin\beta}{m}F_y \\
+\frac{\sin\alpha\cos\beta}{m}F_z + g[\cos\alpha\cos\beta\sin\theta \\
+\sin\beta\sin\phi\cos\theta + \sin\alpha\cos\beta\cos\phi\cos\theta] \\
\dot{p} = \frac{1}{I_{xx}I_{zz}-I_{xz}^2}[(I_{yy}I_{zz} - I_{zz}^2 - I_{xz}^2)rq - I_{xz}(I_{xx} \\
+I_{zz} - I_{yy})pq + I_{zz}L - I_{xz}N] \\
\dot{q} = \frac{1}{I_{yy}}[(I_{zz} - I_{xx})pr + I_{xz}(p^2 - r^2) + M] \\
\dot{r} = \frac{1}{I_{xx}I_{zz}-I_{xz}^2}[(-I_{xx}I_{yy} + I_{zz}^2 + I_{xz}^2)pq \\
+I_{xz}(I_{xx} + I_{zz} - I_{yy})rq + I_{xx}N - I_{xz}L] \\
\dot{\phi} = p + \tan\theta(q\sin\phi + r\cos\phi) \\
\dot{\theta} = q\cos\phi - r\sin\phi \\
\dot{\psi} = \frac{q\sin\phi + r\cos\phi}{\cos\theta}
\end{array}\right\} \quad (1)$$

In (1), $I_{xx}, I_{yy}, I_{zz}, I_{xz}$ are the moments of inertia, m is the mass of the system (kg) and g the gravity constant.u, v, w are translational velocities of the system in body fixed axes in m/s. $\alpha, \beta, V, p, q, r, \phi, \theta, \psi$ are the state variables of the airlaunch aircraft model, they are the angle of attack, sideslip, airspeed, roll rate, pitch rate, yaw rate, roll angle, pitch angle and yaw angle respectively. $\alpha, \beta, \phi, \theta, \psi$ are expressed in rad, p, q, r in rad/s and V in m/s. T is the thrust force, F_x, F_y, F_z and L, M, N are aerodynamic forces and moments respectively. All forces and moments are expressed in N and Nm.

These aerodynamic forces and moments are function of all considered states. In this model, these aerodynamic forces and moments are under look-up table from wind tunnel data measurements as may be found in [9]. Finally, the control inputs are respectively the aileron (δ_a), rudder (δ_r) and elevator (δ_e) angles.

This model is based on wind tunnel data from NASA, considering the following conditions:

- angle of attack is in the range of $[-10°, 45°]$ and sideslip of $[-30°, 30°]$
- flag deflection is ignored
- physical constraints for aileron ($|\delta_a| \leq 21.5°$), rudders ($|\delta_e| \leq 25°$) and elevator ($|\delta_r| \leq 30°$)
- all actuators are modeled as a first order model ($\tau = 1/0.0495s$) with limit rates $60°/s$ for aileron and elevator, and $120°/s$ for rudder.

In particular, we use the low quality mode of the F-16 model, and the aerodynamic data is interpolated and extrapolated linearly in simulation from tables found in [9].

The system was considered starting on an equilibrium point of the first model $(V, h) = (154m/s, 6500m)$, that corresponds to the trimmed angle of attack $\alpha_0 = 12.5°$, pitch angle $\theta_0 = 12.5°$ sideslip $\beta_0 = 0°$, $\phi_0 = 0°$ and to control surface states: aileron $\delta_a = 0°$, elevator $\delta_e = -4.0°$ and rudder $\delta_r = 0°$.

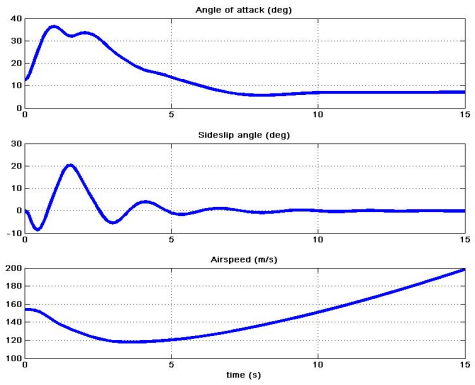

Fig. 3. Angle of attack α, Sideslip β and Airspeed V

We will stabilize the second model following the launch phase to its equilibrium point $(V, h) = (154m/s, 6500m)$, that means angle of attack α_0 to 2.7°, sideslip β to 0°, and roll angle ϕ to 0°.

At first, we take an interval of perturbation $T_{int} = 0.2s$, a simulation of this model with fixed control signals can be seen in Fig. 3. There one can see that the angle of attack and the sideslip are stabilized after the impulsional disturbances on the aerodynamic force and moments. However, Fig. 4 shows that roll angle and pitch angle even if remaining bounded, are not asymptotic stable to their equilibrium at the origin.

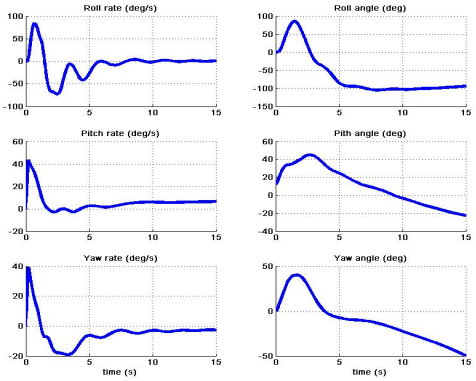

Fig. 4. Outputs stability: Angular Rates and Euler's Angles

If we increase T_{int} to $0.227s$, the system will be completely unstable as shown in Fig. 5.

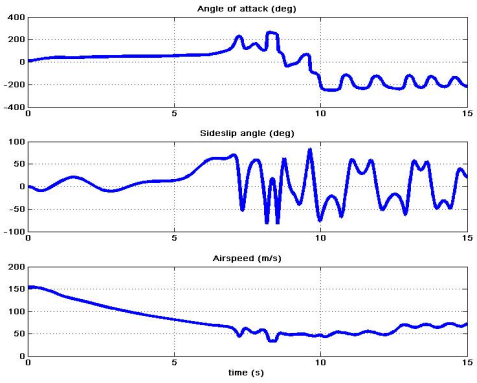

Fig. 5. instability of Angle of attack, Sideslip and Airspeed

III. Control design

A. Conditional integrator control design

The MIMO conditional integrator controller design for the output regulation of a class of minimum-phase nonlinear systems in case of asymptotically constant references is studied in [4], [15] and [16]. These papers concern a servo-compensator performing as a sliding mode controller outside the boundary layer, and performing as a conditional one that provides servo-compensation only inside the boundary layer. First results have studied the SISO case with a scalar sliding surface and the asymptotic stability of the system inside a boundary layer. These results were extended in [14] and [6] for linearized MIMO systems under some additional assumptions. Our present work is dedicated to use a nonlinear extension of these results developed in [2], for stabilizing an unmanned aircraft after the airlaunch phase.

Consider the system:

$$\left\{ \begin{array}{lcl} \dot{e}_1 & = & e_2 \\ \dot{e}_2 & = & f(e_1,e_2)+g(e_1,e_2)u \end{array} \right. \tag{2}$$

where $e_1(t) \in \mathbb{R}^n$ is an output error vector, $e_2 = \dot{e}_1$, $u \in \mathbb{R}^n$ control input and $f(e_1,e_2) \in \mathbb{R}^n$, $g(e_1,e_2) \in \mathbb{R}^{n\times n}$ are continuous functions.

Let us define the sliding surface as:

$$s \quad = \quad k_0\sigma + K_1 e_1 + e_2 \tag{3}$$

where $\sigma \in \mathbb{R}^n$ is the output of the conditional servo-compensator

$$\dot{\sigma} \quad = \quad -k_0\sigma + \mu sat(s/\mu) \tag{4}$$

in which μ is the boundary layer, k_0 is a positive parameter, $K_1 \in \mathbb{R}^{n\times n}$ is chosen such a way that $K_1 + sI_n$ is Hurwitz.

The saturation function is determined as:

$$sat(s/\mu) = \left\{ \begin{array}{ll} s/\|s\| & \text{if } \|s\| \geq \mu \\ s/\mu & \text{if } \|s\| < \mu \end{array} \right. \tag{5}$$

We denote $\mathcal{O}_\mu$ as the region neighborhood of $(e_1,e_2) = (0,0)$ with a radius R_μ for $\|s\| < \mu$

$$\mathcal{O}_\mu \quad = \quad \{e=(e_1,e_2) \in \mathbb{R}^n \times \mathbb{R}^n | \|e\| \leq R_\mu\} \tag{6}$$

We state the following assumptions on the forcing terms $f(e_1,e_2)$ and $g(e_1,e_2)$ to design the control algorithm.

Assumption 3.1: $f(e_1,e_2)$ is bounded by a function $\gamma(e_1,e_2)$ of class $\mathcal{K}$ function and a positive constant F_0

$$\|f(e_1,e_2)\| \leq \gamma(e_1,e_2) + F_0 \tag{7}$$

for $(e_1,e_2) \in \mathbb{R}^n \times \mathbb{R}^n$ and while the sliding surface does not enter the boundary layer, i.e.$\|s\| \geq \mu$.

Inside the boundary layer, the function $f(e_1,e_2)$ is required to be Lipschitz for $(e_1,e_2) \in \mathcal{O}_\mu$, as a consequence

$$\|f(e_1,e_2) - f(0,0)\| \leq L_1\|e_1\| + L_2\|e_2\| \tag{8}$$

where L_1 and $L_2 \in \mathbb{R}^+$.

Assumption 3.2: $g(e_1,e_2)$ satisfies two hypothesis:
Hypothesis 1: for $(e_1,e_2) \in \mathbb{R}^n \times \mathbb{R}^n$

$$g(e_1,e_2) + g^T(e_1,e_2) \geq 2\lambda I_n \text{ with } \lambda > 0 \tag{9}$$

Hypothesis 2: for $(e_1,e_2) \in \mathcal{O}_\mu$, function $g(e_1,e_2)$ is Lipschitz and as a consequence

$$\|g(e_1,e_2) - g(0,0)\| \leq \|g(0,0)\| \upsilon(e_1,e_2) \tag{10}$$

optionally, (10) can be written as

$$\|g(e_1,e_2)g^{-1}(0) - I_n\|\|f(0)\| \quad \leq \quad \upsilon(e_1,e_2) \tag{11}$$

in which, $\upsilon(e_1,e_2)$ is a suitable function satisfying

$$\upsilon(e_1,e_2) \quad = \quad \upsilon_1\|e_1\| + \upsilon_2\|e_2\| \leq K_\upsilon \tag{12}$$

where υ_1, υ_2 and K_υ are suitable positive parameters.

Following these conditions, the controller u defined below in (13) can be applied to (2) to stabilize the system.

$$u = -\Pi(e_1,e_2)sat(s/\mu) \tag{13}$$

in which,

$$\Pi(\cdot) = \Pi_0 + (\gamma(\cdot) + k_0\mu + F_0)/\lambda \tag{14}$$

Π_0, k_0 are positive, μ is the boundary layer as defined above.

When designing this controller, it is important to pay attention that inside the boundary layer, i.e.$\|s\| \leq \mu$, $\Pi(\cdot)$ must satisfy the condition:

$$\Pi(\cdot) - \Pi(0,0) \leq \chi(\cdot) = \lambda\chi_1\|e_1\| + \lambda\chi_2\|e_2\| \tag{15}$$

where χ_1, χ_2 are suitable positive constants and λ was defined earlier in (9).

The stability of the control law (13) for system (2) can be demonstrated following the results of [2].

B. Longitudinal control design

In the longitudinal control design, we assume that all lateral state variables are null or constant, only longitudinal states are time varying. Moreover it is assumed that the airspeed's response is much slower than other states, and that the control surface deflection has no effects on the aerodynamic force components (lift and drag) but only on moments.

Aerodynamic forces F_x, F_z and moment M can be calculated by its aerodynamic coefficients (see more in [5]). $F_x = (C_x(\alpha) + \bar{c}C_{x_q}(\alpha)q/(2V))\bar{q}S$, $F_z = (C_z(\alpha,\beta) + \bar{c}C_{z_q}(\alpha)q/(2V))\bar{q}S$, $M = (C_m(\alpha) + C_{m_q}(\alpha)q\bar{c}/(2V) +$

$C_{m_{\delta_e}}(\alpha)\delta_e)\bar{q}S\bar{c}$. By replacing F_x, F_z, moment M and $\beta = 0$, $\phi = 0$, $p = 0$, $r = 0$ in (1). The model for longitudinal dynamic can be written as:

$$\begin{cases} \dot{\alpha}=\frac{1}{mV}[-\sin\alpha(T+C_x(\alpha)\bar{q}S)+\cos\alpha C_z(\alpha)\bar{q}S] \\ \quad +q+\frac{\rho S}{4m}(-\sin\alpha C_{x_q}(\alpha)\bar{c}+\cos\alpha C_{z_q}(\alpha)\bar{c})q \\ \quad +\frac{g}{V}\cos(\theta_0-\alpha) \\ \dot{q}=I_7\bar{q}S(C_m(\alpha)\bar{c}+C_{m_q}(\alpha)\bar{c}q+C_{m_{\delta_e}}(\alpha)\bar{c}\delta_e) \\ \dot{\theta}=q \end{cases} \tag{16}$$

in which S is wing area, $\bar{q}$ air pressure, $\bar{c}$ equivalent width, $I_7 = 1/I_{yy}$, $C_x(\alpha)$, $C_{x_q}(\alpha)$, $C_z(\alpha)$, $C_{z_q}(\alpha)$, $C_m(\alpha)$, $C_{m_q}(\alpha)$ $C_{m_{\delta_e}}(\alpha)$ are aerodynamic coefficients taken from [7].

Equation (16) can be rearranged as:

$$\begin{cases} \dot{\theta} &= q \\ \dot{\alpha} &= f_{11}^{\alpha}(\alpha)+(1+f_{12}^{\alpha}(\alpha))q+f_{13}^{\alpha}(\alpha,\theta) \\ \dot{q} &= f_{21}^{\alpha}(\alpha)+f_{22}^{\alpha}(\alpha)q+g_2^{\alpha}(\alpha)\delta_e \end{cases} \tag{17}$$

where $f_{11}^{\alpha}(\alpha)$, $f_{12}^{\alpha}(\alpha)$, $f_{13}^{\alpha}(\alpha,\theta)$, $f_{21}^{\alpha}(\alpha)$, $f_{22}^{\alpha}(\alpha)$ and $g_2^{\alpha}(\alpha)$ represent the terms of (16) respectively.

Let us define $x_1^{\alpha} = \alpha$, $x_2^{\alpha} = \dot{x}_1^{\alpha} = \dot{\alpha}$ and $u^{\alpha} = \delta_e$, which allow us to rewrite (17) into:

$$\dot{\theta} = \eta^{\alpha}(x_1^{\alpha}, x_2^{\alpha}, \theta) \tag{18a}$$

$$\dot{x}_1^{\alpha} = x_2^{\alpha}$$

$$\dot{x}_2^{\alpha} = F^{\alpha\prime}(x_1^{\alpha}, x_2^{\alpha}, \theta) + G^{\alpha\prime}(x_1^{\alpha}, x_2^{\alpha})u^{\alpha} \tag{18b}$$

where

$$\begin{cases} \eta^{\alpha}(\cdot) &= (x_2^{\alpha}-f_{11}^{\alpha}(x_1^{\alpha})-f_{13}^{\alpha}(x_1^{\alpha},\theta))/(1+f_{12}^{\alpha}(x_1^{\alpha})) \\ F^{\alpha'}(\cdot) &= \frac{\partial f_{11}^{\alpha}(x_1^{\alpha})}{\partial x_1^{\alpha}}x_2^{\alpha}+\frac{\partial f_{13}^{\alpha}(x_1^{\alpha})}{\partial x_1^{\alpha}}x_2^{\alpha} \\ & \quad +(1+f_{12}^{\alpha}(x_1^{\alpha}))f_{21}^{\alpha}(x_1^{\alpha})+(\frac{\partial(1+f_{12}^{\alpha}(x_1^{\alpha}))}{\partial x_1^{\alpha}}x_2^{\alpha} \\ & \quad +(1+f_{12}^{\alpha}(x_1^{\alpha}))f_{22}^{\alpha}(x_1^{\alpha}))\frac{(x_2^{\alpha}-f_{11}^{\alpha}(x_1^{\alpha})-f_{13}^{\alpha}(x_1^{\alpha}))}{(1+f_{12}^{\alpha}(x_1^{\alpha}))} \\ G^{\alpha'}(\cdot) &= (1+f_{12}^{\alpha}(x_1^{\alpha}))g_2^{\alpha}(x_1^{\alpha}) \end{cases} \tag{19}$$

We define now the reference for the angle of attack α_{ref} considered as constant in this study, and the error vector of angle of attack $e_1^{\alpha} = x_1^{\alpha} - x_{1ref}^{\alpha} = \alpha - \alpha_{ref}$ and the variable $e_2^{\alpha} = \dot{e}_1^{\alpha}$. Equation (18b) can be transformed into (20):

$$\begin{cases} \dot{e}_1^{\alpha} &= e_2^{\alpha} \\ \dot{e}_2^{\alpha} &= F^{\alpha}(e_1^{\alpha}, e_2^{\alpha}, \theta) + G^{\alpha}(e_1^{\alpha}, e_2^{\alpha})u^{\alpha} \end{cases} \tag{20}$$

Here we remark that $G^{\alpha}(x_1^{\alpha}, x_2^{\alpha})$ is invertible, and that $F^{\alpha}(x_1^{\alpha}, x_2^{\alpha}, \theta)$ and $G^{\alpha}(x_1^{\alpha}, x_2^{\alpha})$ are Lipschitz for the entire domain of actuation of the system.

Applying the control algorithm presented in (13) for system (20) (in this case a nonlinear single input single output system) gives the controller:

$$\begin{cases} u^{\alpha} &= -\Pi^{\alpha}(e_1^{\alpha}, e_2^{\alpha})sat(s^{\alpha}/\mu^{\alpha}) \\ \Pi^{\alpha}(\cdot) &= \Pi_0^{\alpha} + (\gamma^{\alpha}(\cdot) + k_0^{\alpha}\mu^{\alpha} + F_0^{\alpha})/\lambda^{\alpha} \end{cases} \tag{21}$$

with

$$\begin{cases} s^{\alpha} = k_0^{\alpha}\sigma^{\alpha} + K_1^{\alpha}e_1^{\alpha} + e_2^{\alpha} \\ \dot{\sigma}^{\alpha} = -k_0^{\alpha}\sigma^{\alpha} + \mu^{\alpha}sat(s^{\alpha}/\mu^{\alpha}) \end{cases} \tag{22}$$

where $\lambda^{\alpha} = min(\|G^{\alpha}(\cdot)\|)$ for $\alpha \in (-10°, 45°)$. Π_0^{α}, μ^{α}, K_1^{α} and k_0^{α} are positive constants.

The controller can be shown to assure the stability of angle of attack and its derivative. For the sake of brevity we skip the proof, that is straightforward and based on a Lyapunov function. It can be shown to go to a residual set that can be attenuated by higher gain. The conclusions we can have are that all errors will be ultimately bounded, where the remaining signals stands for the disturbance on the aircraft speed. It is interesting to remark that variable θ was left free, in order to allow situations as a looping, where θ is continuously varying. Its derivative on the other hand is bounded, and also goes to a residual set (by equation 20).

Since the airspeed control is only a secondary objective, we design a simple PI controller for the thrust to regulate airspeed. Its form is:

$$T = -k_P(V - V_{ref}) - k_I(\dot{V} - \dot{V}_{ref})$$

where V_{ref} is the airspeed reference, $k_P = 1242$ and $k_I = 955$.

C. Lateral control design

As in the case of longitudinal control design, in the lateral case it is considered that only lateral state variables are time varying.

Aerodynamic force F_y and moments L, N are calculated by their aerodynamic coefficients (see more in [5]). $F_y = (C_y(\beta) + (C_{y_p}(\alpha)p + + C_{y_r}(\alpha)r)\bar{b}/(2V))\bar{q}S$, $L = (C_l(\beta) + C_{l_p}(\alpha,\beta)p\bar{b}/(2V) + C_{l_r}(\alpha,\beta)r\bar{b}/(2V) + C_{l_{\delta_a}}(\alpha)\delta_a + C_{l_{\delta_r}}(\alpha)\delta_r)\bar{q}S\bar{b}$, $N = (C_n(\beta) + C_{n_p}(\alpha,\beta)p\bar{b}/(2V) + C_{n_r}(\alpha,\beta)r\bar{b}/(2V) + C_{n_{\delta_a}}(\alpha)\delta_a + C_{n_{\delta_r}}(\alpha)\delta_r)\bar{q}S\bar{b}$. By replacing F_y, moments L, N and $\alpha = \alpha_0$, $\theta = \theta_0$ in (1). The lateral nonlinear dynamic model used for the control design procedure is consequently reduced as below:

$$\begin{cases} \dot{\beta}=\frac{1}{mV}(-\cos(\alpha_0)\sin(\beta)(T+C_x(\alpha_0)\bar{q}S) \\ \quad +\cos(\beta)C_y(\beta)\bar{q}S-\sin(\alpha_0)\sin(\beta)C_z(\alpha_0,\beta)\bar{q}S) \\ \quad +\sin(\alpha_0)p-\cos(\alpha_0)r+\frac{\rho S}{4m}(\cos(\beta)C_{y_p}(\alpha_0)\bar{b}p \\ \quad +\cos(\beta)C_{y_r}(\alpha_0)\bar{b}r)+\frac{g}{V}(\cos(\alpha_0)\sin(\beta)\sin(\theta_0) \\ \quad +\cos(\beta)\cos(\theta_0)\sin(\phi)-\sin(\alpha_0)\sin(\beta)\cos(\phi)) \\ \dot{\phi}=p+\cos(\phi)\tan(\theta_0)r \\ \dot{p}=I_3C_l(\alpha_0,\beta)\bar{q}S\bar{b}+I_4C_n(\alpha_0,\beta)\bar{q}S\bar{b}+\frac{\rho VS\bar{b}}{4}[(I_3C_{l_p}(\alpha_0) \\ \quad +I_4C_{n_p}(\alpha_0))p+(I_3C_{l_r}(\alpha_0)+I_4C_{n_r}(\alpha_0))r] \\ \quad +\bar{q}S[(I_3C_{l_{\delta_a}}(\alpha_0)+I_4C_{n_{\delta_a}}(\alpha_0))\delta_a+(I_3C_{l_{\delta_r}}(\alpha_0) \\ \quad +I_4C_{n_{\delta_r}}(\alpha_0))\delta_r] \\ \dot{r}=I_4C_l(\alpha_0,\beta)\bar{q}S\bar{b}+I_9C_n(\alpha_0,\beta)\bar{q}S\bar{b}+\frac{\rho VS\bar{b}}{4}[(I_4C_{l_p}(\alpha_0) \\ \quad +I_9C_{n_p}(\alpha_0))p+(I_4C_{l_r}(\alpha_0)+I_9C_{n_r}(\alpha_0))r] \\ \quad +\bar{q}S[(I_4C_{l_{\delta_a}}(\alpha_0)+I_9C_{n_{\delta_a}}(\alpha_0))\delta_a+(I_4C_{l_{\delta_r}}(\alpha_0) \\ \quad +I_9C_{n_{\delta_r}}(\alpha_0))\delta_r] \end{cases} \tag{23}$$

In which $\bar{b}$ is equivalent length, $I_3 = \frac{I_{zz}}{(I_{xx}I_{zz}-I_{xz}^2)}$, $I_4 = \frac{I_{xz}}{(I_{xx}I_{zz}-I_{xz}^2)}$, $I_9 = \frac{I_{xx}}{(I_{xx}I_{zz}-I_{xz}^2)}$. $C_y(\alpha,\delta_e)$, $C_{y_p}(\alpha_0)$, $C_{y_r}(\alpha_0)$, $C_l(\alpha_0,\beta)$, $C_n(\alpha_0,\beta)$, $C_{l_p}(\alpha_0)$, $C_{n_p}(\alpha_0)$, $C_{l_r}(\alpha_0)$, $C_{n_r}(\alpha_0)$, $C_{l_{\delta_a}}(\alpha_0)$, $C_{n_{\delta_a}}(\alpha_0)$, $C_{l_{\delta_r}}(\alpha_0)$, $C_{n_{\delta_r}}(\alpha_0)$ are lateral aerodynamic coefficients taken from [7].

Equation (23) can be rearranged as:

$$\begin{cases} \begin{bmatrix}\dot{\beta}\\ \dot{\phi}\end{bmatrix} = f_{11}^{\beta}(\beta,\phi) + f_{12}^{\beta}(\beta,\phi)\begin{bmatrix}p\\ r\end{bmatrix} \\ \begin{bmatrix}\dot{p}\\ \dot{r}\end{bmatrix} = f_{21}^{\beta}(\beta,\phi) + f_{22}^{\beta}(\beta,\phi)\begin{bmatrix}p\\ r\end{bmatrix} + g_2^{\beta}(\beta,\phi)\begin{bmatrix}\delta_a\\ \delta_r\end{bmatrix} \end{cases} \tag{24}$$

where $f_{11}^{\beta}(\cdot)$, $f_{12}^{\beta}(\cdot)$, $f_{13}^{\beta}(\cdot)$, $f_{21}^{\beta}(\cdot)$, $f_{22}^{\beta}(\cdot)$, and $g_2^{\beta}(\cdot)$ represent the terms of (23) respectively. Equation (24) is mainly used for controller design and stability analysis.

Let us define $x_1^{\beta} = [\beta, \phi]^T$, $x_2^{\beta} = \dot{x}_1^{\beta} = [\dot{\beta}, \dot{\phi}]^T$ and $u^{\beta} = (\delta_a, \delta_r)^T$, that allow us to rewrite equation (24) to:

$$\begin{cases} \dot{x}_1^{\beta} &= x_2^{\beta} \\ \dot{x}_2^{\beta} &= F^{\beta'}(x_1^{\beta}, x_2^{\beta}) + G^{\beta'}(x_1^{\beta}, x_2^{\beta})u^{\beta} \end{cases} \tag{25}$$

where

$$\begin{cases} F^{\beta'}(\cdot) = (\frac{\partial f_{11}^{\beta}(\cdot)}{\partial x_1^{\beta}} + (f^{\beta}(\cdot) + f_{12}^{\beta}(\cdot)f_{22}^{\beta}(\cdot))(f_{12}^{\beta}(\cdot))^{-1})x_2^{\beta} \\ -(f^{\beta}(\cdot) + f_{12}^{\beta}(\cdot)f_{22}^{\beta}(\cdot))(f_{12}^{\beta}(\cdot))^{-1}f_{11}^{\beta}(\cdot) + f_{12}^{\beta}(\cdot)f_{21}^{\beta}(\cdot) \\ G^{\beta'}(\cdot) = f_{12}^{\beta}(\cdot)g_2^{\beta}(\cdot) \\ f^{\beta}(\cdot)\,[p, r]^T = \frac{\partial (f_{12}^{\beta}(\cdot)[p,r]^T)}{\partial x_1^{\beta}} \end{cases} \tag{26}$$

We define an output error vector $e_1^{\beta} = x_1^{\beta} - x_{1ref}^{\beta}$ and $e_2^{\beta} = \dot{e}_1^{\beta}$ where $x_{1ref}^{\beta} = (\beta_{ref}, \phi_{ref})^T$ is the output reference considered as constant. Equation (26) can be transformed into (20) with two new state variables e_1^{β} and e_2^{β}.

$$\begin{cases} \dot{e}_1^{\beta} &= e_2^{\beta} \\ \dot{e}_2^{\beta} &= F^{\beta}(e_1^{\beta}, e_2^{\beta}) + G^{\beta}(e_1^{\beta}, e_2^{\beta})u^{\beta} \end{cases} \tag{27}$$

$G^{\beta}(x_1^{\beta}, x_2^{\beta})$ is invertible, and $F^{\beta}(x_1^{\beta}, x_2^{\beta})$ and $G^{\beta}(x_1^{\beta}, x_2^{\beta})$ are Lipschitz in the considered domain of $x_1^{\beta} = [\beta, \phi]^T$, $\dot{x}_1^{\beta} = x_2^{\beta}$ with $\beta \in (-30°, 30°)$ and $\phi \in (-90°, 90°)$.

Application of control law (13) for system (27) leads to the controller:

$$\begin{cases} u^{\beta} &= -\Pi^{\beta}(e_1^{\beta}, e_2^{\beta})sat(s^{\beta}/\mu^{\beta}) \\ \Pi^{\beta}(\cdot) &= \Pi_0^{\beta} + (\gamma^{\beta}(\cdot) + k_0^{\beta}\mu^{\beta} + F_0^{\beta})/\lambda^{\beta} \end{cases} \tag{28}$$

with

$$\begin{cases} s^{\beta} = k_0^{\beta}\sigma^{\beta} + K_1^{\beta}e_1^{\beta} + e_2^{\beta} \\ \dot{\sigma}^{\beta} = -k_0^{\beta}\sigma^{\beta} + \mu^{\beta}sat(s^{\beta}/\mu^{\beta}) \end{cases} \tag{29}$$

where $\lambda^{\beta} = min(\|G^{\beta}(\cdot)\|)$ for $\beta \in (-30°, 30°)$, $\phi \in (-90°, 90°)$. Π_0^{β} is a constant large enough, k_0^{β} is a positive parameter, μ^{β} is the boundary layer and K_1^{β} is a positive definite matrix chosen such a way that $K_1 + sI_2$ is Hurwitz.

IV. Simulation Results

In section III, the design methodology of the conditional integrator controller to stabilize the angle of attack, sideslip and roll angle is proposed when full knowledge of the aerodynamic characteristics is available. This section presents numerical simulation results for the controller to demonstrate the performance of the proposed conditional integrator control laws in the drop phase.

As mentioned in section II, we have considered the launch phase as disturbances on aerodynamic force and moments during a time interval T_{int}, and that the model following the launch phase is that of an F-16. This model is used since it has already been applied for (manned) airlaunch, and because its nonlinear model, wind tunnel informations and data are widely known and used for control design. It is important to remark that the model used in the following simulations is even more complete than that used in the control design, for example it includes actuator dynamics and their limitations. As a consequence, simulations also illustrate some properties of robustness to unmodeled dynamics.

In the following simulations, we have simultaneously applied the SISO longitudinal controller for angle of attack, and the MIMO lateral one for the sideslip and roll angles in the full nonlinear F-16 aircraft model. We may note that the control inputs are limited by their physical limitations introduced in section II.

The control law in (14) whose $\Pi(\cdot)$ can be written more simply as:

$$\Pi(\cdot) = \Pi_0 + \gamma(\cdot) \tag{30}$$

in which, $\gamma(\cdot) = \gamma_1\|e_1\|^2 + \gamma_2\|e_2\|^2$, γ_1 and γ_2 are positive constant.

Application of this control law to two motion modes presented in subsections (III-B) and (III-C) is done by determining the set of parameters Π_0^i, γ_1^i, γ_2^i, μ^i, K_1^i and k_0^i with $i = \alpha, \beta$ corresponding to longitudinal mode and lateral mode respectively. We use the design parameters in the Table I for the longitudinal controller, and the design parameters in Table II for the lateral controller. In Table II, Π_0^{β} and k_0^{β} are defined in matrix form because of the difference in the dynamic property of two state variables *sideslip* and *roll angle*. This definition does not have any consequence on the stability of the system.

Π_0^{α}	μ^{α}	γ_1^{α} and γ_2^{α}	k_0^{α}	K_1^{α}
25.0	1.0	0.1 and 0.1	2.0	2.0

TABLE I

Parameters for the longitudinal mode

Π_0^{β}	μ^{β}	γ_1^{β} and γ_2^{β}	k_0^{β}	K_1^{β}
$\begin{bmatrix} 10 & 0.0 \\ 0.0 & 15 \end{bmatrix}$	1.0	0.01 and 0.01	$\begin{bmatrix} 1.5 & 0.0 \\ 0.0 & 1.5 \end{bmatrix}$	$\begin{bmatrix} 2.0 & 0.0 \\ 0.0 & 2.0 \end{bmatrix}$

TABLE II

Parameters for the lateral mode

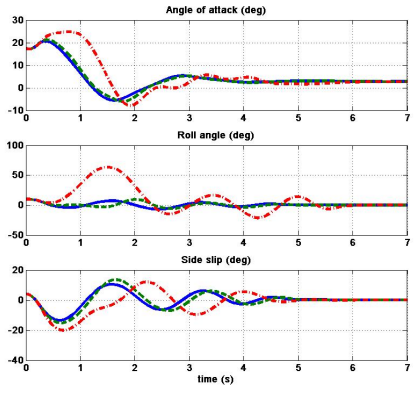

Fig. 6. System Output: Angle of attack, Sideslip Angle and Roll angle stabilized

We will stabilize the second model following the launch phase to its equilibrium point $(V, h) = (154m/s, 6500m)$ corresponding to (angle of attack α_r to 2.7°, sideslip β_r to 0°, and roll angle ϕ_r to 0°).

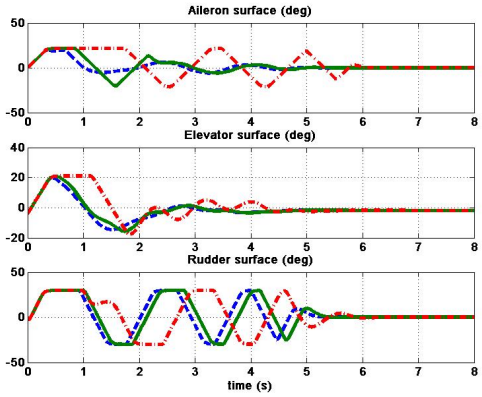

Fig. 7. Control surface: Aileron, Elevator and Rudder

Its initial condition is the final state of the first model ($\alpha = 12.5°$, $\beta = 0°$ and $\phi = 0°$) as in Section II. Moreover, we add on its initial condition a small disturbance on system output. That means the initial condition of second model is ($\alpha_0 = 17.5°$, $\beta_0 = 4°$ and $\phi_0 = 10°$) for all numerical simulations.

The second model is disturbed on its aerodynamic force and moments during an interval T_{int} as in Section II.

We simulate three sets of time lengths. $T_{int} = 0.2s$ (corresponding to solid lines in Fig. 6 to Fig. 8) produces damped oscilations. In the case with $T_{int} = 0.227s$, it was shown in Section II that the uncontrolled system become completely unstable. In this case the Conditional Integrator is able to stabilize the system as can be seen in the dashed lines in Fig. 6 to Fig. 8. When $T_{int} = 0.3s$ (corresponding to dash dotted lines in Fig. 6 to Fig. 8) one can see that the controller is still able to stabilize the system.

Fig. 6 illustrates the convergence of the system output to the operating point of the aircraft at the end of 5s without static steady error for the three cases of $T_{int} = (0.2s, 0.227s, 0.3s)$. All system outputs are still under their physical limitation.

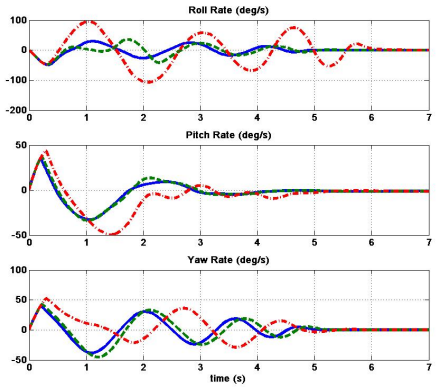

Fig. 8. State variables: Angular rates of system

Figs. 8 shows that angular rates converge to zero in all cases.

In Fig. 7, it can be seen that the control variables are saturated by their physical limitations due to a high perturbation on aerodynamic forces and moments.

Finally we show in Fig. 9 and Fig. 10 that the system will be unstable even with the robust conditional integrator controller for an interval $T_{int} = 0.4s$.

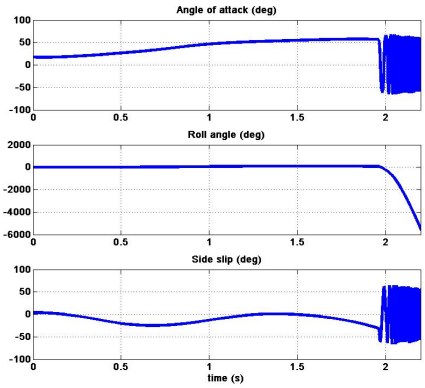

Fig. 9. Angle of attack, Sideslip Angle and Roll angle unstable

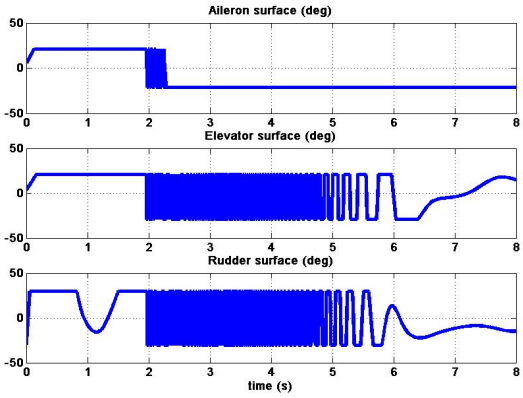

Fig. 10. Saturation of Aileron, Elevator and Rudder

Collision Avoidance

Airlaunch problem does not only require stability of system's states, but also to avoid the possibility of collision between the aircraft and the rocket after the drop phase. Fig. 11 shows the altitude of the aircraft from 0 to $1s$ in the three previous cases of study $T_{int} = (0.2s, 0.227s, 0.3s)$. They are compared with the trajectory of the rocket that drop freely with the initial airspeed of the aircraft (the solid plot). It is important to remark that there is a small distance from the initial height of the rocket and the aircraft, representing the distance between the aircraft and the rocket.

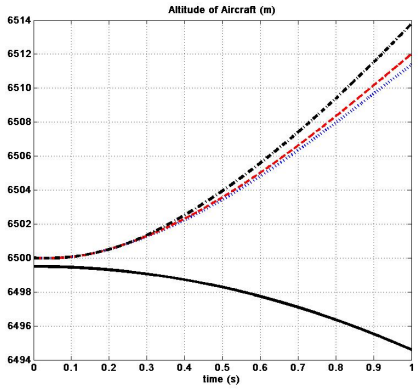

Fig. 11. Altitude of the aircraft

In the three cases (dotted plot, dashed plot and dash dotted plot), the altitude of the aircraft satisfies the specification that requires there is no collision between the aircraft and the rocket in the airlaunch phase.

V. Conclusion

We have introduced the modeling and simulation of an airlaunch system at the stage separation from the reusable airlaunch vehicle from the down stage. This work has studied the effects of the staging phase in the stability of the airlaunch system. Because our airlaunch system have a down stage mass close to the launch vehicle's one, the separation phase produces large changes in aerodynamic force and moment, as demonstrated in section II, which may turn the system unstable. These changes may, specially in the case of a non perfect separation phase, produce large impulses on forces and moments, making the system unstable. These impulses are considered to last a time interval, that is then evaluated in simulations.

To stabilize the airlaunch system after this stage separation phase, a conditional integrator control is considered. This controller is designed using an F-16 model representing the aircraft just after dropping the second stage, but disturbed by large impulses.

For a perturbation on aerodynamic forces and moments during an interval T_{int}, the stability of the system after the drop stage may be assured for small time intervals. When T_{int} becomes large, the system becomes unstable even with the proposed controller.

In future works other disturbances will be considered, as well as other control strategies for this particularly interesting and difficult problem. The objective being to perform flight tests in a near future.

References

[1] M.M. Burlacu and J. Kohlenberg. An analysis of the nanosatellites launches between 2004 and 2007. *3rd International Conference on Systems and Networks Communications*, pages 292–297, 2008.

[2] Gilney Damm and Van Cuong Nguyen. Mimo conditional integrator control for a class of nonlinear systems. *Journal of Control Engineering and Applied Informatics; Buletinul Institutului Politehnic din Iasi; Annals of the University of Craiova; The Annals of "Dunarea de Jos" University of Galati*, 2011.

[3] Gary C. Hudson. Quickreach responsive launch system. *American Institute of Aeronautics and Astronautics*, 2006.

[4] Hassan K. Khalil. On the design of robust servomechanisms for minimum phase nonlinear systems. *Robust Nonlinear Control 2000, John Wiley & Sons*, 10:339–361, 2000.

[5] Taeyoung Lee and Youdan Kim. Nonlinear adaptive flight control using backstepping and neural networks controller. *Journal of guidance, control and dynamics*, 24:675–682, 2001.

[6] Attaullah Y. Memona and Hassan K. Khalil. Output regulation of nonlinear systems using conditional servocompensators. *Automatica*, 2010.

[7] Eugene Morelli. Global nonlinear parametric modeling with application to f-16 aerodynamics. *American Institute of Aeronautics and Astronautics*, 1998.

[8] J. Christophe Naftel and Richard Powell. Analysis of the staging maneuver and booster glideback guidance for a two-stage, winged, fully reusable launch vehicle. *NASA Technical Paper*, 1993.

[9] L.T. Nguyen, M.E. Ogburn, and P. Deal. Simulator study of fighter airplane with relaxed longitudinal static stability. *Technical report NASA*, page 1538, 1979.

[10] Bandu N. Pamadi, Thomas A. Neirynck, and Peter F. Covell. Simulation and analyses of staging maneuvers of next generation reusable launch vehicles. *American Institute of Aeronautics and Astronautics*, 2004.

[11] Bandu N. Pamadi, Thomas A. Neirynck, and Peter F. Covell. Simulation and analyses of staging maneuvers of next generation reusable launch vehicles. *American Institute of Aeronautics and Astronautics*, 2004.

[12] Bandu N. Pamadi, Thomas A. Neirynck, and Nathaniel J. Hotchko. Simulation and analyses of stage separation of two-stage reusable launch vehicles. *AIAA/CIRA 13th International Space Planes and Hypersonics Systems and Technologies*, 2005.

[13] Marti Sarigul-Klijn and Nesrin Sarigul-Klijn. Selection of a carrier aircraft and a launch method for air launching space vehicles. *American Institute of Aeronautics and Astronautics*, 2008.

[14] Sridhar Seshagiri and Hassan K. Khalil. Robust output feedback regulation of minimum-phase nonlinear systems using conditional integrators. *Automatica*, 2004.

[15] Sridhar Seshagiri and Hassan K. Khalil. Robust output feedback regulation of minimum-phase nonlinear systems usingconditional integrators. *Automatica*, 2005.

[16] Sridhar Seshagiri and Hassan K. Khalil. Robust output regulation of minimum phase nonlinear systems using conditional servocompensators. *Wiley InterScience*, 2005.

[17] Lars Sonneveldt. *Nonlinear F-16 Model Description*. Delft University of Technology, Netherlands, 2006.

[18] Peter H. Zipfel. *Modeling and Simulation of Aerospace Vehicle Dynamics, 2nd edition*. American Institute of Aeronautics and Astronautics, 2000.